Three-phase threshold capillary pressures in noncircular capillary tubes with different wettabilities including contact angle hysteresis

Mohammad Piri* and Martin J. Blunt
Department of Earth Science and Engineering, Imperial College, London SW7 2AZ, United Kingdom
(Received 10 July 2004; revised manuscript received 5 October 2004; published 14 December 2004)

We use the Helmholtz free energy balance and the Mayer-Stowe-Princen method to derive general expressions governing multiphase pistonlike displacements in noncircular capillary elements with arbitrary wettability. We take into account hysteresis in oil/water, gas/water, and gas/oil contact angles. We study both two- and three-phase systems. We find threshold capillary pressures for gas invasion into oil, oil invasion into gas, and water invasion into oil for capillaries with an irregular triangular cross section. Finally we study the effects of shape factor, oil/water capillary pressure, and oil/water and gas/oil contact angles on the threshold capillary pressure for gas invasion into oil for spreading and nonspreading systems. In many cases the threshold pressures of the three-phase displacements are not the same as those of the equivalent pseudo-two-phase displacements. It is possible that gas invasion can occur resulting in a configuration without oil layers, even if oil layers are geometrically possible. This emphasizes the distinction between geometric and thermodynamic stability—it is the latter that controls threshold pressures.

DOI: 10.1103/PhysRevE.70.061603 PACS number(s): 68.08.Bc, 47.55.Mh

I. INTRODUCTION

Understanding multiphase flow in porous media is important in many areas of science and technology including petroleum reservoir and environmental engineering. One appealing approach to calculate macroscopic multiphase flow properties, such as relative permeability and capillary pressure, is physically based pore-scale network modeling where the pore space is described as a network of pores connected by throats with some idealized geometry. Then a series of displacement steps in each pore or throat (element) are combined to simulate multiphase flow. Recent advances in pore-scale modeling have been reviewed by Celia *et al.* [1], Blunt [2], and Blunt *et al.* [3].

Individual pores and throats are often considered to have angular cross sections; see, for instance, [4–7]. This makes it possible to have more than one phase residing in one element; the wetting phase occupies the corners when the nonwetting phase fills the center. As well as triangular cross-sectional elements [4–7], authors have used geometries with circular [8], square [9–11], star-shaped [12,13], and lenticular [14] cross sections to represent pores and throats.

Displacements of one phase by another in capillaries with different cross-sectional shapes, wettability, and inscribed radius are distinguished from each other by their threshold capillary pressures. There are different types of displacement: pistonlike, pore-body filling, snap-off, and layer formation and collapse [6,15–17]. Here we consider only pistonlike displacement, which refers to the displacement of one phase by another in the center of a throat by a fluid residing in the center of a neighboring pore. The threshold capillary pressures are found using the Mayer-Stowe-Princen (MSP) method [18–21]; see Sec. IV for details.

The MSP method has been applied by several authors to compute threshold capillary pressures for pistonlike displacement in elements with circular and different angular cross sections [5,15,22–24]. Øren *et al.* [6] and Patzek [7] have studied two-phase displacements in irregular triangles with arbitrary contact angles. Lago and Araujo [25,26] extended this work to consider two-phase flow in capillaries with polygonal cross sections and curved sides. Van Dijke *et al.* [27–29] found three-phase threshold capillary pressures in elements with noncircular cross sections and different wettability but ignored wettability alteration and contact angle hysteresis.

In this paper we compute threshold capillary pressures for three-phase pistonlike displacements in polygonal cross-sectional elements. The difference between this and other work is that we study three-phase flow with altered wettability surfaces taking into account hysteresis in oil/water, gas/water, and gas/oil contact angles.

We first give an introduction to pistonlike displacement, wettability alteration, and contact angle hysteresis. Then a brief description of the MSP method is presented which is followed by developing a Helmholtz free energy balance in closed systems where phases are separated by spherical interfaces. The free energy balance equation is used to derive the general threshold capillary pressure equations for three-phase pistonlike drainage and imbibition in noncircular cross-section capillaries with n corners of arbitrary wettability. A special case where capillaries are irregular triangles in cross section is considered to find threshold capillary pressures for gas invasion into oil, oil invasion into gas, and water invasion into oil in strongly oil-wet systems taking into account contact angle hysteresis. The sensitivity of threshold capillary pressures to shape factor and other capillary pressures is also studied.

II. PRESSURE DIFFERENCE ACROSS AN INTERFACE

To find the pressure difference across an interface, we use the Young-Laplace equation [30,31]

*Present address: Department of Civil and Environmental Engineering, Engineering Quad E-228, Princeton University, Princeton, NJ 08544, USA. Electronic address: mpiri@princeton.edu

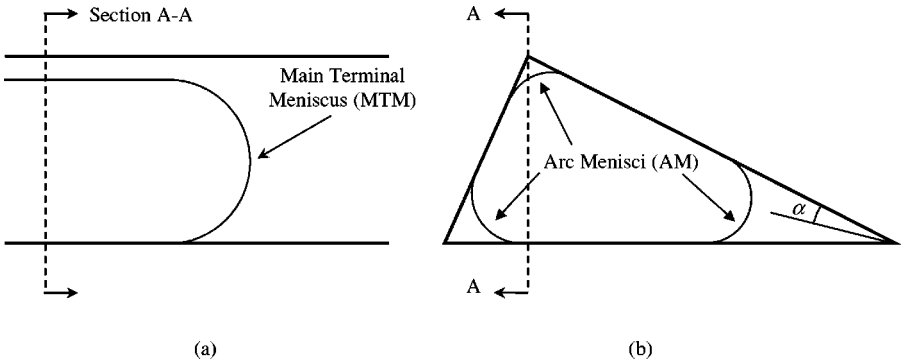

FIG. 1. Different types of interface (a) main terminal meniscus (MTM), and (b) arc menisci (AMs) in the corners of a capillary element of triangular cross section. α is the corner half angle [5].

$$P_i - P_j = \sigma_{ij}\left(\frac{1}{r_1} + \frac{1}{r_2}\right) \tag{1}$$

where r_1 and r_2 are the principal radii of curvature, and P_i and P_j are pressures of the phases on either sides of the interface.

There are two types of interface, Fig. 1. The first is the *main terminal meniscus* (MTM) [5], which is the invading meniscus at the pore/throat junction separating wetting and nonwetting fluids in the center of the pore and throat. The shape of such a meniscus is usually assumed to be spherical, meaning that the two radii of curvature are the same ($r_1 = r_2 = r$). The second type are the *arc menisci* (AMs), which are the interfaces at corners of a noncircular element usually left by a pistonlike displacement (see Sec. III). It is assumed that the curvature of the interface is negligible in the plane perpendicular to that of the paper meaning that the principal radii of curvature would be $r_1 = r$ and $r_2 = \infty$ [5,30]. The pressure difference across such an interface is given by

$$P_i - P_j = \frac{\sigma_{ij}}{r}. \tag{2}$$

The capillary pressure P_{cij} is simply the pressure difference across the interface:

$$P_{cij} = P_i - P_j. \tag{3}$$

III. PISTONLIKE DISPLACEMENT

Pistonlike displacement refers to the displacement of one phase by another in the center of a throat by a fluid residing in the center of a neighboring pore. In other words, once the threshold capillary pressure is reached the MTM that has access to the entrance of the element moves into the capillary with a fixed curvature filling the center of the element by the invading phase. While the MTM displaces the defending phase *k* from the center of the element—in *noncircular* elements—the residual of the displaced phase may remain in the corners, creating new AMs. This happens only if

$$\theta_k^* < \frac{\pi}{2} - \alpha \tag{4}$$

where θ_k^* is the angle that the new AMs make with the solid surface toward the apex of the corner which may or may not be the contact angle that is traditionally measured through the denser phase, and α is the corner half angle [see Fig. 1(b)]. If the effects of gravity are ignored then the curvature of the AMs will be exactly the same as that of the invading MTM [5].

Every displacement is either drainage or imbibition. *Drainage* in a capillary element refers to an event where a wetting phase is displaced by a nonwetting phase. An event in which a nonwetting phase is displaced by a wetting phase is called *imbibition*. Pistonlike displacement can take place in both cases. The prevailing contact angles during pistonlike drainage and imbibition events are receding and advancing values, respectively (see Sec. III A). If there is no contact angle hysteresis then the threshold capillary pressure of pistonlike imbibition is the same as that of drainage; otherwise during imbibition the relevant capillary pressure is reduced and each interface starts hinging from its furthest value toward the advancing contact angle. It stays pinned as long as the hinging value is smaller than the advancing contact angle. The wetting phase will enter the element when the advancing contact angle is reached. The threshold capillary pressures are found using the Mayer-Stowe-Princen method described in Sec. IV.

A. Wettability alteration and contact angle hysteresis

While most clean rock surfaces in contact with refined oils are water wet, few, if any, oil reservoirs are completely water wet. This is because of direct contact of crude oil with the solid surface which changes its wettability by adsorption of polar components of the crude oil or the presence of naturally oil-wet minerals within the rock. This makes any values of oil/water and consequently gas/water and gas/oil contact angles possible [32–36]. Kovscek *et al.* [34] developed a model where the wettability of the rock surface is assumed to be altered by the direct contact of oil. Before a porous medium is invaded by oil it is assumed to be full of water and water wet. Once it is invaded by oil a thin film of water prevents oil touching the solid surface directly. But at a threshold capillary pressure this film can rupture and allows oil to contact the solid surface and change its wettability. Regions of the pore space not contacted by oil remain water wet.

The contact angle also depends on the direction of displacement. This difference between *advancing*, i.e., a wetting phase displacing the nonwetting one, and *receding*, i.e., a nonwetting phase displacing the wetting one, contact angles

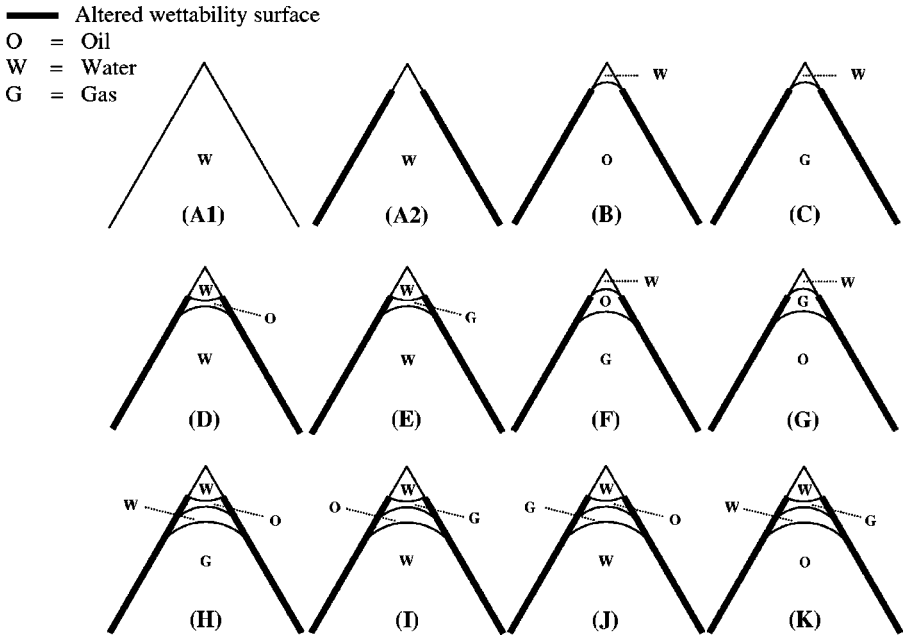

FIG. 2. One-, two-, and three-phase configurations for a single corner. The bold solid line indicates regions of the surface with altered wettability. All the multiphase contact points may be pinned which means that, as the capillary pressure changes, the curvature of the interface changes but that the location of the interface/solid contact is fixed. It can move only when the hinging contact angle becomes equal to the pertinent contact angle. A phase may be present in the center of the pore space or as a spreading or wetting layer, sandwiched between other phases. Water is always present in the corner.

may be as large as 50°–90° [30,37,38] depending on surface roughness, surface heterogeneity, swelling, rearrangement, or alteration of the surface by solvent [30].

Different oil/water, gas/water, and gas/oil contact angles and interfacial tensions make it theoretically possible to accommodate fluids in the corners of the pore space with different configurations. Figure 2 illustrates possible generic configurations of one, two, or three fluids in a single corner of an angular pore or throat [17]. Altered wettability surfaces are shown by thicker lines.

IV. MAYER-STOWE-PRINCEN METHOD

The MSP method is based on equating the pressure difference across the AMs left at the corners of the capillary tube by pistonlike displacement, which is given by Eq. (2) for elements with straight walls, to that of the MTM which is found by writing an energy balance for MTM invasion (see Sec. IV A).

A. Helmholtz free energy balance

Imagine a closed system where two strictly homogeneous phases i and j are precisely separated by a flexible spherical *dividing* surface with zero thickness, radius r, and area A [39,40]. Since the interface is not plane the uniform pressure of bulk phase i, P_i, is different from that of j, P_j. If the volumes of the two phases, V_i and V_j, in mechanical equilibrium are changed by variation in state variables of the system by $dV=dV_i=-dV_j$, causing a reversible change in A, dA, the work dW carried out by the system to do such a change is given by

$$dW = P_i dV_i + P_j dV_j - \sigma_{ij} dA_{ij} \tag{5}$$

where σ_{ij} is the interfacial tension for the Gibbs surface of tension and is the work done per unit increase in interfacial area [39,40].

If the radius of the surface of tension is much larger than thickness of the interface then interfacial tension can be considered independent of the radius of the dividing surface [39] and is uniform in all directions. Knowing that, the pressure difference across the interface is related to the interfacial tension by

$$P_i - P_j = \frac{2\sigma_{ij}}{r} \tag{6}$$

which is the famous Laplace-Kelvin equation for a spherical interface.

The change in the area of the interface changes the internal energy of the system, dU, which is related to dW using the first law of thermodynamics:

$$dU = dQ - P_i dV_i - P_j dV_j + \sigma_{ij} dA_{ij} \tag{7}$$

where dQ is the heat given to the system. If the system is in thermodynamic equilibrium then using the second law of thermodynamics Eq. (7) can be rewritten as

$$dU = TdS - P_i dV_i - P_j dV_j + \sigma_{ij} dA_{ij} \tag{8}$$

where T is the temperature of the system and S is the entropy. Then the change in Helmholtz free energy, dF, is given by

$$dF = -SdT - P_i dV_i - P_j dV_j + \sigma_{ij} dA_{ij}. \tag{9}$$

One should note that we consider only closed systems, meaning that the composition of the system is fixed. Also there is no exchange of molecules between the phases—we consider completely immiscible systems.

The total Helmholtz free energy of the system can be considered as the summation of Helmholtz free energy of the two bulk phases i and j, and the interface

$$F = F_i + F_j + F_{interface}. \tag{10}$$

Equation (9) for bulk phases i and j in a system with constant temperature becomes

$$dF_i = -P_i dV_i, \tag{11}$$

$$dF_j = -P_j dV_j. \tag{12}$$

From Eqs. (9)–(12) we obtain

$$dF_{interface} = \sigma_{ij} dA_{ij}. \tag{13}$$

Extension of the above analysis for an n-phase system with the same conditions gives

$$dF = -\sum_{i=1}^{j=n} P_i dV_i + \sum_{ij=12,13,\ldots,23,24,\ldots}^{n!/2(n-2)!} \sigma_{ij} dA_{ij}. \tag{14}$$

A system with constant temperature and constant total volume is at equilibrium when the Helmholtz free energy F is minimum [41] or

$$dF = 0. \tag{15}$$

B. Capillary systems with three fluid phases

Consider a noncircular capillary element with n corners filled with defending phase in the center and invading phase having access at one end of it where it forms a MTM. An increase in the pressure of the invading phase to the threshold value when the pressure of the defending phase is fixed results in the MTM entering the capillary with a fixed curvature and changing fluid configurations (old to new) at the corners. Assuming that the system is closed, at equilibrium, the MTM spherical, the solid (s) a rigid phase ($dV_s=0$), and the solid walls straight, for a small movement dx of a MTM in the capillary where three fluids, i.e., oil (o), water (w), and gas (g), may be present, the Helmholtz free energy balance can be written using Eqs. (14) and (15):

$$dF = -\sum_{i=o,w,g} P_i dV_i + \sum_{ij=ow,os,go,gs,gw,ws} \sigma_{ij} dA_{ij} = 0, \tag{16}$$

where

$$dV_i = \{[A_{i,t}\delta_i]^{nc} - [A_{i,t}\delta_i]^{oc}\}dx = \left\{\sum_{k=1}^{n} [A_{i,\measuredangle_k}\delta_{i,\measuredangle_k}]^{nc} - [A_{i,\measuredangle_k}\delta_{i,\measuredangle_k}]^{oc}\right\}dx, \tag{17}$$

$$dA_{ij} = \{[L_{ij,t}\delta_{ij}]^{nc} - [L_{ij,t}\delta_{ij}]^{oc}\}dx = \left\{\sum_{k=1}^{n} [L_{ij,\measuredangle_k}\delta_{ij,\measuredangle_k}]^{nc} - [L_{ij,\measuredangle_k}\delta_{ij,\measuredangle_k}]^{oc}\right\}dx, \tag{18}$$

where the subscripts nc and oc stand for new and old configurations, respectively, $A_{i,t}$ is the total area occupied by phase i in the cross section, $L_{ij,t}$ is the total length of contact between phases i and j in the cross section, n is the number of corners in the cross section, and $\measuredangle_k$ is the corner k (see Fig. 3 for an example). If phase i is present in a cross section then δ_i is 1; otherwise it is zero. Also when phases i and j have an interface together then δ_{ij} is 1; otherwise it is zero. The same analogy applies in a corner for $\delta_{i,\measuredangle_k}$ and $\delta_{ij,\measuredangle_k}$.

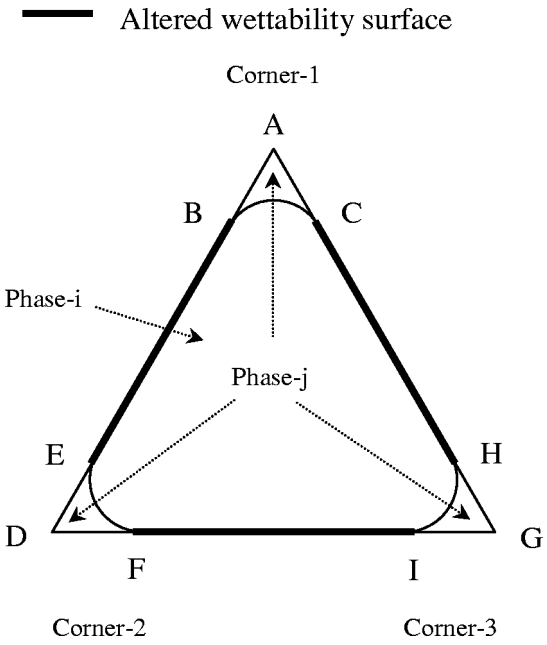

FIG. 3. Different areas and contact lengths in an equilateral triangle with a two-phase configuration: $A_{j,\measuredangle_1}=A_{ABC}$, $A_{j,\measuredangle_2}=A_{DEF}$, $A_{j,\measuredangle_3}=A_{GHI}$, $L_{ij,\measuredangle_1}=BC$, $L_{ij,\measuredangle_2}=EF$, $L_{ij,\measuredangle_3}=HI$, $L_{js,\measuredangle_1}=2AB$, $L_{js,\measuredangle_2}=2DE$, $L_{js,\measuredangle_3}=2GH$, $L_{js,t}=\Sigma_{k=1}^{3}L_{js,\measuredangle_k}$, $L_{is,t}=L-L_{js,t}$, $A_{j,t}=\Sigma_{k=1}^{3}A_{j,\measuredangle_k}$, and $A_{i,t}=A-A_{j,t}$.

The total area of the cross section A_t and the perimeter L_t of the capillary are constant and given by

$$A_t = \sum_{i=o,w,g} A_{i,t}\delta_i, \tag{19}$$

$$L_t = \sum_{i=o,g,w} L_{is,t}\delta_{is}. \tag{20}$$

From Eqs. (16)–(18) the comprehensive form of Helmholtz free energy balance is

$$-\sum_{i=o,w,g} P_i \sum_{k=1}^{n} \{[A_{i,\measuredangle_k}\delta_{i,\measuredangle_k}]^{nc} - [A_{i,\measuredangle_k}\delta_{i,\measuredangle_k}]^{oc}\} + \sum_{ij=ow,os,go,gs,gw,ws} \sigma_{ij} \sum_{k=1}^{n} \{[L_{ij,\measuredangle_k}\delta_{ij,\measuredangle_k}]^{nc} - [L_{ij,\measuredangle_k}\delta_{ij,\measuredangle_k}]^{oc}\} = 0. \tag{21}$$

When two fluids i and j come in contact on a solid surface s, where the solid is continuous at the line of contact, then according to Young, Laplace [31], and Gibbs [40] the force balance parallel to the surface at equilibrium becomes

$$\sigma_{ij}\cos\theta_{ij} = \sigma_{is} - \sigma_{js} \tag{22}$$

where θ_{ij} is the angle measured through phase j which is traditionally taken to be the denser phase.

In a three-phase system Eq. (22) can be written for each of the three pairs of fluids, i.e., oil-water, gas-water, and gas-oil, residing on a solid surface

$$\sigma_{os} - \sigma_{ws} = \sigma_{ow}\cos\theta_{ow}, \tag{23}$$

$$\sigma_{gs} - \sigma_{ws} = \sigma_{gw} \cos \theta_{gw}, \tag{24}$$

$$\sigma_{gs} - \sigma_{os} = \sigma_{go} \cos \theta_{go}. \tag{25}$$

A constraint on the three-phase contact angles and interfacial tensions in mutual equilibrium can be derived by manipulation of Eqs. (23)–(25) [42,43]:

$$\sigma_{gw}^{eq} \cos \theta_{gw} = \sigma_{go}^{eq} \cos \theta_{go} + \sigma_{ow}^{eq} \cos \theta_{ow}. \tag{26}$$

Equation (26) means that in three-phase systems only two of the contact angles need to be defined independently. Generalization of this analysis to a system with n fluid phases was shown by Blunt [44] where there are $n(n-1)/2$ contact angles, $(n-1)(n-2)/2$ constraints, and $(n-1)$ independent contact angles.

In this work we use Eq. (26) to find the dependent contact angle. We first decide on the values of two of the contact angles and then calculate the third one using Eq. (26). We use θ_{ow}^{r} and θ_{go}^{r} to calculate a θ_{gw}. We also use θ_{ow}^{a} and θ_{go}^{a} to find another value of θ_{gw}. The smaller of the two values of θ_{gw} is considered as the receding and the larger one as the advancing value.

In three-phase systems the three capillary pressures between three pairs of fluids are related as

$$P_{cgw} = P_{cgo} + P_{cow}. \tag{27}$$

Equations (21) and (23)–(27) are used to find the pressure difference across the MTM which is then set equal to the pressure difference across the appropriate AM to find threshold capillary pressures for any pistonlike displacement in two- and three-phase systems. Next we present some examples.

V. EXAMPLE: IRREGULAR TRIANGLES

Other authors have used the general energy balance Eq. (16) to derive threshold capillary pressures [25–28]. In this work we will apply it to study two- and three-phase displacements for the configurations in Fig. 2 that have not been studied before.

Here as an example we use capillaries with irregular triangular cross sections to find threshold capillary pressures for different two- and three-phase pistonlike displacements. Appendix A presents useful geometrical relationships for irregular triangles.

A. Gas invasion into oil

Imagine an irregular triangle with configuration B (old configuration), Fig. 2, in all three corners. Displacement of oil in the center of the capillary by gas will form either configuration F and/or C (new configurations) at each corner depending on whether the oil layer is stable. Using Eqs. (2), (19), (20), (24), (25), and (27), Eq. (21) can be written as

$$P_{cgo} = \frac{\sigma_{go}}{r_{go}} = \frac{P_{cow}\sum_{k=1}^{3}[(A_{w,\measuredangle_k}\delta_{w,\measuredangle_k})^{nc} - (A_{w,\measuredangle_k}\delta_{w,\measuredangle_k})^{oc}] + \sigma_{ow}\zeta_{ow} + \sigma_{go}\zeta_{go} + \sigma_{gw}\zeta_{gw}}{[(A_{g,t}\delta_g)^{nc} - (A_{g,t}\delta_g)^{oc}]} \tag{28}$$

where

$$\zeta_{ow} = \sum_{k=1}^{3}[(L_{ow,\measuredangle_k}\delta_{ow,\measuredangle_k})^{nc} - (L_{ow,\measuredangle_k}\delta_{ow,\measuredangle_k})^{oc}], \tag{29}$$

$$\zeta_{go} = \sum_{k=1}^{3}\{[(L_{go,\measuredangle_k}\delta_{go,\measuredangle_k})^{nc} - (L_{go,\measuredangle_k}\delta_{go,\measuredangle_k})^{oc}] - [(L_{os,\measuredangle_k}\delta_{os,\measuredangle_k})^{nc} - (L_{os,\measuredangle_k}\delta_{os,\measuredangle_k})^{oc}]\cos\theta_{go}^{r}\}, \tag{30}$$

$$\zeta_{gw} = \sum_{k=1}^{3}\{[(L_{gw,\measuredangle_k}\delta_{gw,\measuredangle_k})^{nc} - (L_{gw,\measuredangle_k}\delta_{gw,\measuredangle_k})^{oc}] - [(L_{ws,\measuredangle_k}\delta_{ws,\measuredangle_k})^{nc} - (L_{ws,\measuredangle_k}\delta_{ws,\measuredangle_k})^{oc}]\cos\theta_{gw}^{r}\}, \tag{31}$$

where for this set of configuration changes $(\delta_g)^{oc}=0$, $(\delta_g)^{nc}=1$, $(\delta_{w,\measuredangle_k})^{nc(oc)}=1$, $(\delta_{ow,\measuredangle_k})^{oc}=1$, $(\delta_{go,\measuredangle_k})^{oc}=0$, $(\delta_{os,\measuredangle_k})^{oc}=1$, $(\delta_{gw,\measuredangle_k})^{oc}=0$, and $(\delta_{ws,\measuredangle_k})^{nc(oc)}=1$ for $k=1,2,3$.

Whether the pistonlike displacement leaves an oil layer in a corner depends on if Eq. (4) holds for $\theta_k^*=\theta_{go}^r$ and if it does, then whether the layer is stable. For a given P_{cow} an oil layer in corner k is stable only if the inequality given by Eq. (C24) (see Appendix C) holds with $ij=go$, $jk=ow$, $\theta_k^*=\theta_w^*$, and $\theta_j^*=\theta_{go}^r$.

Different areas and lengths in Eqs. (28)–(31) are given by

$$(A_{g,t})^{nc} = \left\{\frac{R^2}{4G} - \sum_{k=1}^{3}[(A_{o,\measuredangle_k} + A_{w,\measuredangle_k})\delta_{o,\measuredangle_k}]^{nc} - \sum_{k=1}^{3}[A_{w,\measuredangle_k}(1-\delta_{o,\measuredangle_k})]^{nc}\right\} \tag{32}$$

where R is the inscribed radius, G is the shape factor (see

Appendix A), and $[A_{o,\measuredangle_k}+A_{w,\measuredangle_k}]^{nc}$ is given by Eq. (B9) (see Appendix B), with $r_{jk}=r_{go}$ and $\theta_k^*=\theta_{go}^r$. If water in the corner is in contact with the gas in the center $(A_{w,\measuredangle_k})^{nc}$ is found using the same equation with r_{gw} and θ_{gw}^r, otherwise, to find $(A_{w,\measuredangle_k})^{nc(oc)}r_{ow}$ and θ_w^* are used instead.

$(L_{ow,\measuredangle_k})^{nc(oc)}$ is computed from Eq. (B10) (see Appendix B), with $r_{jk}=r_{ow}$ and $\theta_k^*=\theta_w^*$. Using the same equation we find $(L_{go,\measuredangle_k})^{nc}$ with r_{go} and θ_{go}^r and $(L_{gw,\measuredangle_k})^{nc}$ with r_{gw} and θ_{gw}^r.

The differences between the lengths of solid in contact with oil and water in *oc* and *nc* are as follows:

$$\sum_{k=1}^{3}[(L_{os,\measuredangle_k}\delta_{os,\measuredangle_k})^{nc}-(L_{os,\measuredangle_k})^{oc}] = \left\{2\sum_{k=1}^{3}[(b_{o,\measuredangle_k}-b_{w,\measuredangle_k})\delta_{o,\measuredangle_k}]^{nc}\right\} - \left\{\frac{R}{2G}-2\sum_{k=1}^{3}(b_{w,\measuredangle_k})^{oc}\right\}, \tag{33}$$

$$\sum_{k=1}^{3}[(L_{ws,\measuredangle_k})^{nc}-(L_{ws,\measuredangle_k})^{oc}]=2\sum_{k=1}^{3}[(b_{w,\measuredangle_k})^{nc}-(b_{w,\measuredangle_k})^{oc}] \tag{34}$$

where in the corners with oil layer, configuration *F*, b_o is given by Eq. (B3) (see Appendix B), with $r_{jk}=r_{go}$ and $\theta_k^*=\theta_{go}^r$. Also b_w of the oil/water interface is calculated using the same equation with r_{ow}^{ext} and θ_w^*, where r_{ow}^{ext} is the extremum oil/water radius of curvature reached during the process by which this interface was moved last time. If there is any corner where gas in the center is in direct contact with water then b_w is found using r_{gw} and θ_{gw}^r instead.

In order to find the threshold capillary pressure of the displacement for a given P_{cow} an iterative procedure is used. First a P_{cgo} is guessed, then, using Eq. (4) and the layer stability analysis given in Appendix C, we can find if the oil layers are stable in the corners; then a new P_{cgo} is calculated using Eq. (28). If this is not close enough to the one we guessed then it is used for the next round of calculations by checking the stability of the oil layers with this new P_{cgo}. Iteration continues until the difference between two consecutive values of P_{cgo} becomes less than a predefined small value.

If oil layers are stable in all corners separating water from gas, then $(A_{w,t})^{nc}-(A_{w,t})^{oc}=0$, $\zeta_{ow}=0$, $\zeta_{gw}=0$, and $-(L_{gs,t})^{nc}=[(L_{os,t})^{nc}-(L_{os,t})^{oc}]$ which reduces Eq. (28) to

$$P_{cgo}=\frac{\sigma_{go}}{r_{go}}=\frac{\sigma_{go}[L_{go,t}+L_{gs,t}\cos\theta_{go}^r]^{nc}}{(A_{g,t})^{nc}} \tag{35}$$

which represents the well-known expression for threshold capillary pressure of two-phase pistonlike displacement [6,25] which indicates that, in this case, the threshold gas/oil capillary pressure is independent of the oil/water capillary pressure. This is similar to the work by van Dijke and Sorbie [27].

One should note that in this work water, if Eq. (4) holds for $\theta_k^*=\theta_w^*$, is present in the corner as a wetting layer regardless of the oil/water contact angle of the altered wettability surfaces. This is not the case, for instance, in the three-phase work by van Dijke and Sorbie [27].

In the above calculations we have allowed oil layers to form in the corners if they are stable; see Eq. (4) and Appendix C. But one may argue (see, for instance, van Dijke *et al.* [28,29]), that this may not be a sufficient criterion for allowing the oil layers to form, meaning that not allowing the oil layers to form even if they are stable may give lower threshold gas/oil capillary pressures. In order to make sure the threshold gas/oil capillary pressure that we present in each case is the lowest possible, we also calculate the threshold gas/oil capillary pressure of gas invasion into oil without allowing oil layers to form, even if they are stable. Then we compare it with the one we calculated allowing oil layers. The one which is smaller is favored; see Sec. IV for examples.

B. Oil invasion into gas

Invasion of oil into gas in a triangle with configurations *C* and/or *F* at the corners will result in the formation of configurations *B* and/or *G* depending on gas/oil and oil/water contact angles and capillary pressures. We consider this process immediately after gas invasion into oil. Similar to the previous section using Eqs. (2), (19), (20), (23), (25), and (27). Eq. (21) can be written as

$$P_{cgo}=\frac{\sigma_{go}}{r_{go}}=\frac{-P_{cgw}\sum_{k=1}^{3}[(A_{w,\measuredangle_k}\delta_{w,\measuredangle_k})^{nc}-(A_{w,\measuredangle_k}\delta_{w,\measuredangle_k})^{oc}]-\sigma_{ow}\zeta_{ow}-\sigma_{go}\zeta_{go}-\sigma_{gw}\zeta_{gw}}{[(A_{o,t}\delta_o)^{nc}-(A_{o,t}\delta_o)^{oc}]}, \tag{36}$$

$$\zeta_{ow}=\sum_{k=1}^{3}\{[(L_{ow,\measuredangle_k}\delta_{ow,\measuredangle_k})^{nc}-(L_{ow,\measuredangle_k}\delta_{ow,\measuredangle_k})^{oc}]-[(L_{ws,\measuredangle_k}\delta_{ws,\measuredangle_k})^{nc}-(L_{ws,\measuredangle_k}\delta_{ws,\measuredangle_k})^{oc}]\cos\theta_{ow}^r\}, \tag{37}$$

$$\zeta_{go}=\sum_{k=1}^{3}\{[(L_{go,\measuredangle_k}\delta_{go,\measuredangle_k})^{nc}-(L_{go,\measuredangle_k}\delta_{go,\measuredangle_k})^{oc}]+[(L_{gs,\measuredangle_k}\delta_{gs,\measuredangle_k})^{nc}-(L_{gs,\measuredangle_k}\delta_{gs,\measuredangle_k})^{oc}]\cos\theta_{go}^a\}, \tag{38}$$

$$\zeta_{gw} = \sum_{k=1}^{3} [(L_{gw,\measuredangle_k}\delta_{gw,\measuredangle_k})^{nc} - (L_{gw,\measuredangle_k}\delta_{gw,\measuredangle_k})^{oc}], \quad (39)$$

where for this set of configuration changes $(\delta_o)^{nc}=1$, $(\delta_{gs,\measuredangle_k})^{oc}=1$, $(\delta_{w,\measuredangle_k})^{nc(oc)}=1$, and $(\delta_{ws,\measuredangle_k})^{nc(oc)}=1$ for $k=1,2,3$.

If Eq. (4) holds for $\theta_k^* = \pi - \theta_{go}^a$ then after oil invasion it is possible to have gas layers sandwiched between water in the corners and oil in the center but only if they are stable. For a known P_{cgw} a gas layer in corner k is stable only if the inequality given by Eq. (C23) (see Appendix C) holds with $ij=go$, $jk=gw$, $\theta_k^*=\theta_w^*$, and $\theta_j^* = \pi - \theta_{go}^a$.

For this set of configuration changes, i.e., displacement, different areas and lengths used in Eqs. (36)–(39) are given by

$$(A_{o,t})^{nc} = \frac{R^2}{4G} - \left\{ \sum_{k=1}^{3} [(A_{g,\measuredangle_k} + A_{w,\measuredangle_k})\delta_{g,\measuredangle_k}]^{nc} + [A_{w,\measuredangle_k}(1-\delta_{g,\measuredangle_k})]^{nc} \right\}, \quad (40)$$

$$(A_{o,t})^{oc} = \sum_{k=1}^{3} \{[(A_{o,\measuredangle_k} + A_{w,\measuredangle_k})\delta_{o,\measuredangle_k}]^{oc} - (A_{w,\measuredangle_k}\delta_{o,\measuredangle_k})^{oc}\}, \quad (41)$$

where $(A_{g,\measuredangle_k}+A_{w,\measuredangle_k})^{nc}$ is calculated using Eq. (B9) with $r_{jk}=r_{go}$ and $\theta_k^*=\pi-\theta_{go}^a$. $(A_{w,\measuredangle_k})^{nc}$ in the corners with a gas layer, configuration *G*, is found using the same equation with r_{gw} and θ_w^*. But if the water in the corner is in contact with the oil in the center then the water area is calculated using r_{ow} and θ_{ow}^r instead. Calculation of areas in the old configurations has been discussed in the previous section, configurations *F* and *C*.

In the new configurations, i.e., *B* and *G*, $(L_{ow,\measuredangle_k})^{nc}$ is found using Eq. (B10) with $r_{jk}=r_{ow}$ and $\theta_k^*=\theta_{ow}^r$. Similarly in the corners where there is a gas layer we find $(L_{go,\measuredangle_k})^{nc}$ with r_{go} and $\pi-\theta_{go}^a$ and $(L_{gw,\measuredangle_k})^{nc}$ with r_{gw} and θ_w^*. The calculation of lengths for different interfaces in the old configurations has been discussed in the previous section, configurations *F* and *C*,

$$\sum_{k=1}^{3} [(L_{gs,\measuredangle_k}\delta_{gs,\measuredangle_k})^{nc} - (L_{gs,\measuredangle_k})^{oc}] = 2\sum_{k=1}^{3} [(b_{g,\measuredangle_k} - b_{w,\measuredangle_k})\delta_{g,\measuredangle_k}]^{nc} - \left\{ \frac{R}{2G} - 2\sum_{k=1}^{3} \{(b_{o,\measuredangle_k}\delta_{o,\measuredangle_k})^{oc} + [b_{w,\measuredangle_k}(1-\delta_{o,\measuredangle_k})]^{oc}\} \right\} \quad (42)$$

where in the corners with a gas layer, b_g is given by Eq. (B3) with $r_{jk}=r_{go}$ and $\theta_k^*=\pi-\theta_{go}^a$. Also b_w of the gas/water interface in the new configuration is calculated using the same equation with r_{gw}^{ext} and θ_w^*, where r_{gw}^{ext} is the extremum gas/water radius of curvature reached during the process by which the interface was moved last time. If there is any corner where water is in direct contact with the oil in the center then b_w is found using the same equation with r_{ow} and θ_{ow}^r. Calculation of the meniscus-apex distance for the different interfaces in the old configurations has been discussed in the previous section. Also the difference between the lengths of solid in contact with water in *nc* and *oc* is given by Eq. (34).

The threshold gas/oil capillary pressure is found using an iterative procedure. At a given P_{cgw}, a gas/oil capillary pressure is guessed, where $r_{go}=\sigma_{go}/P_{cgo}$, and a new P_{cgo} is calculated using Eq. (27). Then if there is any corner with configuration *F*, the *hinging* gas/oil contact angle for gas/oil interface is calculated from

$$\theta_{go,\measuredangle_k}^h = \cos^{-1}\left[\frac{r_{go}^{ext}}{r_{go}}\cos(\theta_{go}^r + \alpha_{\measuredangle_k})\right] - \alpha_{\measuredangle_k} \quad (43)$$

where r_{go}^{ext} is the radius of curvature by which the interface moved last time. Since we are considering oil invasion into oil after gas invasion into gas, this is the minimum radius of curvature reached during the gas invasion. If $\theta_{go,\measuredangle_k}^h > \theta_{go}^a$ then $\theta_{go,\measuredangle_k}^h = \theta_{go}^a$ otherwise we use $\theta_{go,\measuredangle_k}^h$ itself for the calculations. Then $b_{o,\measuredangle_k}$ is calculated using Eq. (B3) with $r_{jk}=r_{go}^{ext}$ and $\theta^*=\theta_{go}^r$, if $\theta_{go,\measuredangle_k}^h < \theta_{go}^a$; otherwise with r_{go} and θ_{go}^a.

One should note that when it comes to calculating the length of a gas/oil interface in a corner with an oil layer, configuration *F*, Eq. (B10) (see Appendix B) is used with $r_{jk}=r_{go}$ and $\theta^*=\theta_{go}^a$, if $\theta_{go,\measuredangle_k}^h > \theta_{go}^a$; otherwise with $\varphi_{\measuredangle_k} = \sin^{-1}[(b_{o,\measuredangle_k}\sin\alpha_{\measuredangle_k})/r_{go}]$.

Now we find if a gas layer can form in any of the corners using the procedure discussed earlier in this section. Then using Eqs. (28)–(39) a new P_{cgo} is calculated. This iterative process continues until the difference between two consecutive values of P_{cgo} is less than a predefined small value.

Again, to make sure that the threshold gas/oil capillary pressure calculated is the highest possible, a threshold gas/oil capillary pressure is calculated without the gas layers being allowed to form even if they are stable. Then it is compared with the one that is calculated allowing the gas layers to form, if they are stable, and then the one that is greater is favored.

C. Water invasion into oil in a strongly oil-wet element

Here we present a set of equations to find the threshold capillary pressure for water invasion into oil in a strongly oil-wet capillary element changing configuration *B* in each corner to either *D* (if the oil layer is stable) or *A*2 (otherwise); see Fig. 2. It is a two-phase pistonlike displacement so Eq. (21) reduces to

TABLE I. Interfacial tensions and spreading coefficient (mN/m) used in this work [45,46].

Set no.	Fluids	σ_{ow}	σ_{go}	σ_{gw}	C_s
I	Hexane-water-air	48	19	67	0
II	Dodecane-water-air	52.3	25.35	72	−5.65

$$P_{cow} = \frac{\sigma_{ow}}{r_{ow}} = \frac{\sigma_{ow}\{[(L_{ow}^{co} + L_{ow}^{lce})^{nc} - (L_{ow}^{co})^{oc}] + [(L_{ws}^{co} + L_{ws}^{ce})^{nc} - (L_{ws}^{co})^{oc}]\cos\theta_{ow}^{a}\}}{(A_{w}^{co} + A_{w}^{ce})^{nc} - (A_{w}^{co})^{oc}} \tag{44}$$

where the superscripts *lce*, *ce*, and *co* stand for layer center, center, and corner, and $(L_{ow}^{lce})^{nc}$ is the total length of the contact line between oil in the layer(s) and water in the center and is found using Eq. (B10) with $r_{jk}=r_{ow}$ and $\theta_k^*=\pi-\theta_{ow}^a$. $(L_{ws}^{ce})^{nc}$ is the total length of contact between water in the center and solid walls and is given by

$$(L_{ws}^{ce})^{nc} = \frac{R}{2G} - 2\sum_{k=1}^{3}(b_{o,\measuredangle_k}\delta_{o,\measuredangle_k})^{nc} \tag{45}$$

where $(b_{o,\measuredangle_k})^{nc}$ is given by Eq. (B3) using $r_{jk}=r_{ow}$ and $\theta_k^*=\pi-\theta_{ow}^a$.

$(A_w^{ce})^{nc}$ is the area of water in the center which is found from

$$(A_w^{ce})^{nc} = \frac{R^2}{4G} - \sum_{k=1}^{3}[(A_{o,\measuredangle_k} + A_{w,\measuredangle_k}^{co})\delta_{o,\measuredangle_k}]^{nc} \tag{46}$$

where $[A_{o,\measuredangle_k}+A_{w,\measuredangle_k}^{co}]^{nc}$ is computed from Eq. (B9) using $r_{jk}=r_{ow}$ and $\theta_k^*=\pi-\theta_{ow}^a$.

In this displacement, an oil layer can be left in corner k only if $\theta_{ow}^a \geq \pi/2+\alpha_{\measuredangle_k}$; see Eq. (4) with $\theta_k^*=\pi-\theta_{ow}^a$. If this condition holds then an oil layer will form only if it is stable. Stability of a layer sandwiched between two identical fluids has been analyzed in Appendix C 1.

Similar to the procedure used in Sec. V A, a P_{cow} is guessed then using Eq. (C21) with $jk=ow$, $j=o$, and $k=w$ we calculate the threshold capillary pressure of oil layer collapse in each corner. If the threshold capillary pressure of oil layer collapse is larger than the guessed P_{cow} then it will not form. Then a new P_{cow} is computed from Eq. (44) knowing the configuration of each corner. If the difference between computed and guessed P_{cow} is smaller than a predefined small value then that is the final threshold capillary pressure otherwise it is used as a new guess for P_{cow} and iteration continues.

Similar to two previous sections, threshold oil/water capillary pressure without letting the oil layers to form, even if they are stable, is also calculated and compared with the threshold capillary pressure that was calculated allowing the oil layers to form if they are stable. The one that is greater is favored.

VI. SENSITIVITY ANALYSIS

Here we study the sensitivity of threshold capillary pressures for the case discussed in Sec. V A (gas invasion into oil) to the shape factor of an irregular triangle G, oil/water capillary pressure P_{cow}, advancing oil/water contact angle θ_{ow}^a, and receding gas/oil contact angle θ_{go}^r.

An irregular triangle is considered with an inscribed radius of 13.6 μm, which is the average inscribed radius of the network used by Piri and Blunt [17] as representative of Berea sandstone. The pore is assumed to be full of water and water-wet initially. Then oil invades into water by an increase in oil/water capillary pressure to some threshold value [6,7,17,47]. The prevailing contact angle during this process, primary drainage θ_{ow}^{PD}, is considered to be zero. The oil/water capillary pressure is then increased to 10^5 Pa. Oil now is in contact with the solid walls and may change the wettability. Knowing the interfacial tensions (see Table I), and using the procedure described in Sec. IV B, five sets of receding and advancing contact angles are assigned to the pore (see Table II).

Then water flooding is modeled by decreasing oil/water capillary pressure during which the oil/water contact angle starts hinging from θ_{ow}^{PD} toward θ_{ow}^a. The hinging contact angle $\theta_{ow,\measuredangle_k}^h$ is calculated using Eq. (43) with r_{ow}^{ext}, r_{ow}, and θ_{ow}^r. The reduction in oil/water capillary pressure is continued only to values larger than the threshold oil/water capillary pressure for water invasion into oil which ranges from 6200 to −6800 Pa for the different systems tabulated in Table II [6,7,17]. This is because we do not want to invade the pore by water. As will be shown later, we decrease the oil/water capillary pressure only to enable us to study the effects of oil/water capillary pressure and hinging oil/water contact angles on the threshold gas/oil capillary pressure of tertiary gas invasion into oil.

The shape factor is varied between 0.005 and $\sqrt{3}/36$. For each triangle the corner half angles are found using the

TABLE II. Contact angles (deg) used in the sensitivity analysis.

System	IFT set	θ_{ow}^{PD}	θ_{ow}^r	θ_{ow}^a	θ_{go}^r	θ_{go}^a	θ_{gw}^r	θ_{gw}^a
A	I	0	10	30	0	0	8.46	25.31
B	I	0	160	180	0	0	112.93	115.65
C	II	0	10	30	40	60	9.91	36.38
D	II	0	10	30	60	80	26.95	46.35
E	II	0	160	180	60	80	120.43	131.70

TABLE III. Corner half angles (deg) for irregular triangles with different shape factors

G	$\alpha_{\measuredangle_1}$	$\alpha_{\measuredangle_2}$	$\alpha_{\measuredangle_3}$
0.005	1.215	24.643	64.141
0.01	2.565	25.388	62.047
0.015	4.096	26.094	59.811
0.02	5.794	26.793	57.412
0.025	7.739	27.469	54.792
0.03	10.034	28.116	51.850
0.035	12.756	28.749	48.495
0.04	16.199	29.341	44.46
0.0481	30	30	30

method described in Appendix A. Table III tabulates the corner half angles used in this work.

Now gas invasion into oil is carried out by increasing the gas/oil capillary pressure. The iterative procedure described in Sec. V A is used to find threshold gas/oil capillary pressures for pistonlike displacement of oil by gas. For each system given in Table II the sensitivity of the threshold gas/oil capillary pressure is examined to the shape factor and oil/water capillary pressure.

Figures 4 and 5 show the variation of threshold gas/oil capillary pressure with shape factor for systems *A* and *B* (see Table II), respectively. The threshold gas/oil capillary pressures for two scenarios, with and without oil layers, are shown. For the range of shape factor and oil/water capillary pressure used the scenario with oil layers is strictly favored, lower threshold gas/oil capillary pressure, which is similar for both systems and not sensitive to the variation in oil/water capillary pressure since oil layers are present in all three corners (see Fig. 9 below). This is purely a two-phase displacement since there is no gas/water interface in the cross sections. The oil layers are present since the gas/oil capillary pressures required to collapse the layers are greater than the threshold gas/oil capillary pressure of the pistonlike displacement.

Figures 6 and 7 illustrate the behavior of the threshold gas/oil capillary pressure for two scenarios, with and without oil layers, due to variations in oil/water capillary pressure and shape factor for systems *C* and *D*, respectively. The scenario without oil layers is favored only for low oil/water capillary pressures and large shape factors where it gives lower threshold gas/oil capillary pressures than those of the scenario with oil layers. The scenario with oil layers produces threshold gas/oil capillary pressures that are relatively insensitive to P_{cow} except for very low oil/water capillary pressures in large shape factor triangles, where layers in some or all of the corners do not form. For instance, the sharp drop in threshold gas/oil capillary pressure for a triangle with $G=0.04$ can be seen in Fig. 7 for $P_{cow}=10\,000$ Pa is due to the fact that there are no oil layers in any of the corners separating gas and water. The other triangles have at least, for this particular system and oil/water capillary pressure, one oil layer. For both systems *C* and *D* the route for high oil/water capillary pressure presents, approximately, the two-phase threshold capillary pressure as most of the corners have oil layers separating gas in the center from the water in the corner.

Figure 8 indicates the sensitivity of threshold gas/oil capillary pressure to oil/water capillary pressure and shape factor for system *E* for both scenarios, with and without oil layers. The scenario with oil layers is strictly favored since it gives lower threshold gas/oil capillary pressures. As it is tabulated in Table II, the gas/water contact angle for this system is larger than 90°, making $\cos\theta_{gw}$, in Eq. (31), negative in comparison to system *D* where it was positive. Threshold gas/oil capillary pressures for this system are sensitive to both oil/water capillary pressure and shape factor. Similar to system *D*, ζ_{ow} [see Eq. (29)] is more negative for fewer corner configurations with oil layers but all the other terms in the numerator of Eq. (28) are larger for lower oil/water capillary pressure giving larger threshold gas/oil capillary pressures with a greater sensitivity to P_{cow}. This was

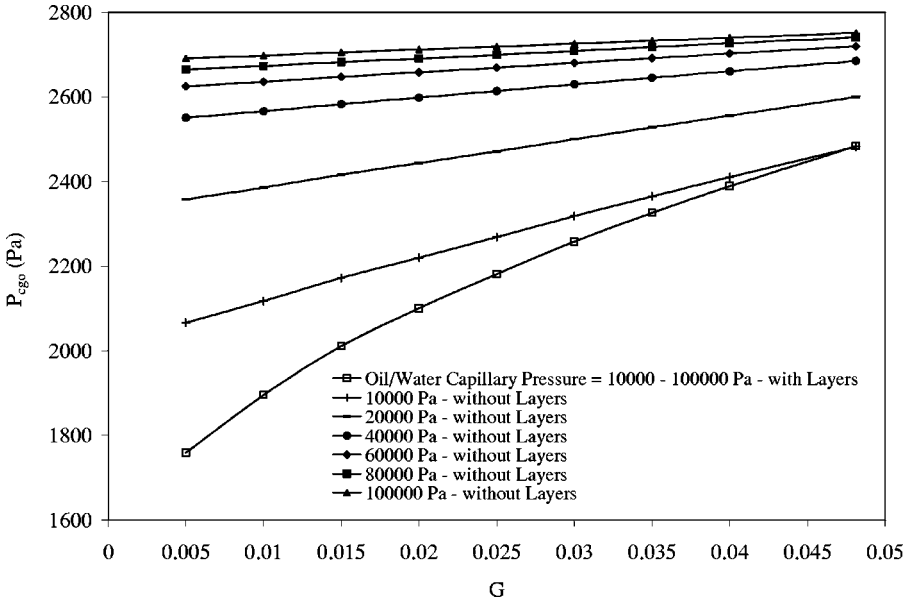

FIG. 4. Threshold gas/oil capillary pressures for system *A*.

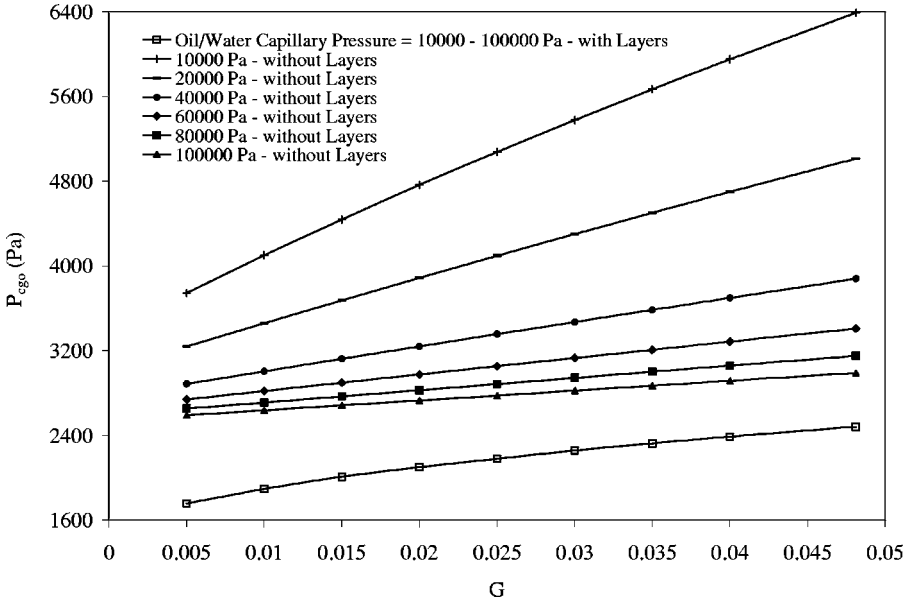

FIG. 5. Threshold gas/oil capillary pressures for system *B*.

not the case in system *D*, for instance (Fig. 7). The lower limit of the envelope, high oil/water capillary pressures and low shape factors, approximately presents the two-phase threshold capillary pressures as the oil layers are present in most of the corners.

As mentioned earlier, during gas invasion into oil, configuration *F* may form in all or some of the corners depending on the pertinent capillary pressures and contact angles. Figures 9–11 show the variation of the ratio $\sigma_{ow}P_{cgo}/\sigma_{go}P_{cow}$ with changes in corner half angle and gas/oil and oil/water contact angles (see Appendix C 2) for the equations used to produce the figures. One can use these figures to find if the oil layers are stable in different corners of a triangle in the systems discussed above. For a given gas/oil contact angle, oil/water contact angle, and corner half angle, one can find the ratio $\sigma_{ow}P_{cgo}/\sigma_{go}P_{cow}$. Then knowing the interfacial tensions and oil/water capillary pressure, a gas/oil capillary pressure can be obtained which, if is less than the threshold gas/oil capillary pressure shows that the oil layer in that particular corner does not exist.

VII. DISCUSSION AND CONCLUSIONS

We used the Helmholtz free energy balance and the MSP method to derive a general expression to calculate the threshold capillary pressures of two- and three-phase pistonlike displacements. Each displacement was modeled as a configuration change in the corners of a capillary with angular cross section. Using different two- and three-phase generic configurations we were able to study any piston-like displacement. Adopting the wettablity alteration scenario developed by Kovscek *et al.* [34] enabled us to take into account contact angle hysteresis in threshold capillary pressure calculations. This scenario also allowed us to leave water at the corners regardless of the oil/water contact angle of the altered wettability surface, which was not the case in previous

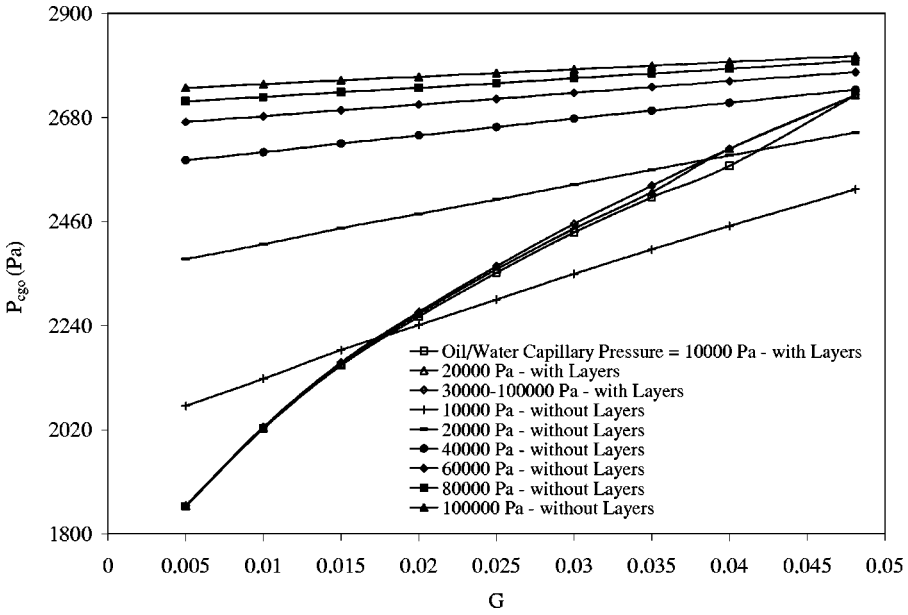

FIG. 6. Threshold gas/oil capillary pressures for system *C*.

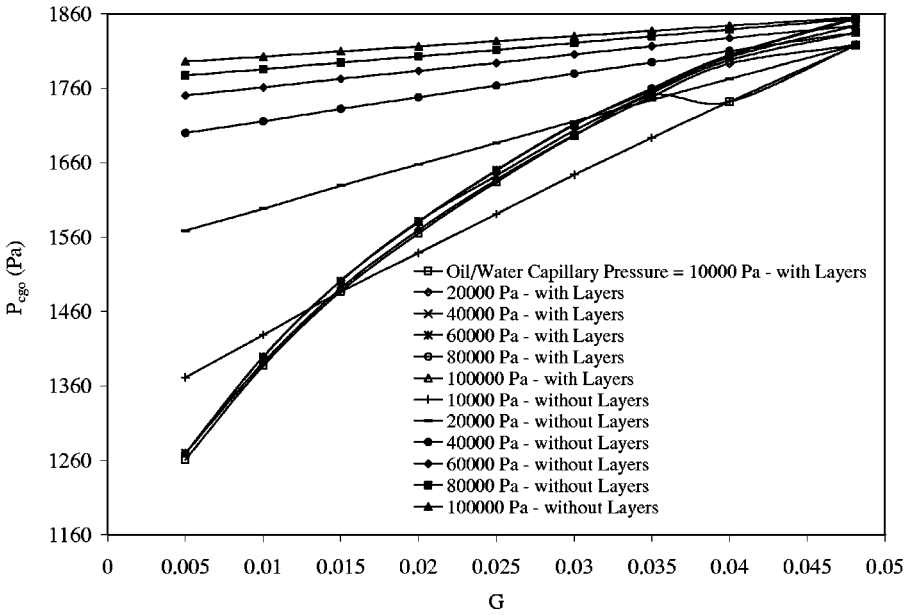

FIG. 7. Threshold gas/oil capillary pressures for system *D*.

work, for instance, by van Dijke and Sorbie [27,28].

The procedure of using the general expression to find the threshold capillary pressures of three different displacements, i.e., gas invasion into oil, oil invasion into gas, and water invasion into oil in strongly oil-wet systems, was presented. Then we studied the sensitivity of the threshold gas/oil capillary pressure for tertiary gas invasion into oil on the shape factor for capillaries with irregular triangular cross sections for different oil/water capillary pressures. We carried out the sensitivity analysis for spreading and nonspreading oils in five systems with different wettabilities. In each case in order to make sure that the calculated threshold capillary pressure of the pistonlike displacement presents the lowest threshold pressure of the invading phase, we did the calculations for two scenarios: (I) layers of the displaced phase were allowed to form in the corners if they were stable; and (II) layers were not allowed to form even if they were stable. The one with the lower pressure of the invading phase was favored. Scenario I was strictly favored in systems *A* and *B* where oil was spreading. But this was not necessarily the case in systems with nonspreading oil, *C* and *D*, except in the strongly oil-wet case *E*.

We found that the threshold gas/oil capillary pressure is sensitive to the shape factor so that the lower the shape factor the lower the threshold gas/oil capillary pressure. But this was not necessarily the case for the oil/water capillary pressure. Threshold capillary pressures for scenario II were always sensitive to oil/water capillary pressure since gas and water were in contact in all the corners. But for scenario I, if oil remains in all the corners as layers to separate gas in the center from the water in the corners, then the threshold gas/oil capillary pressure is insensitive to oil/water capillary pressure, similar to the case of van Dijke and Sorbie [27], which is likely to be the case in the spreading systems *A* and

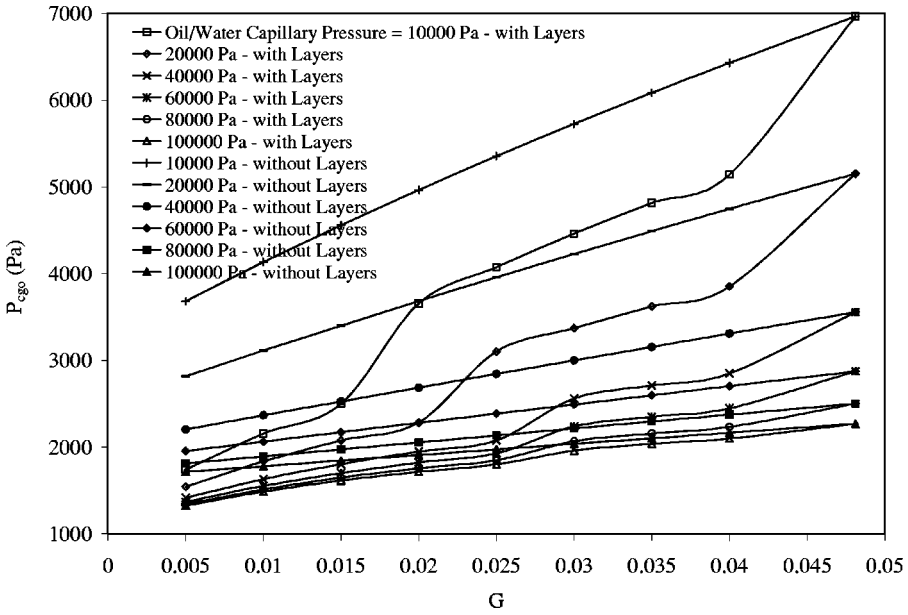

FIG. 8. Threshold gas/oil capillary pressures for system *E*.

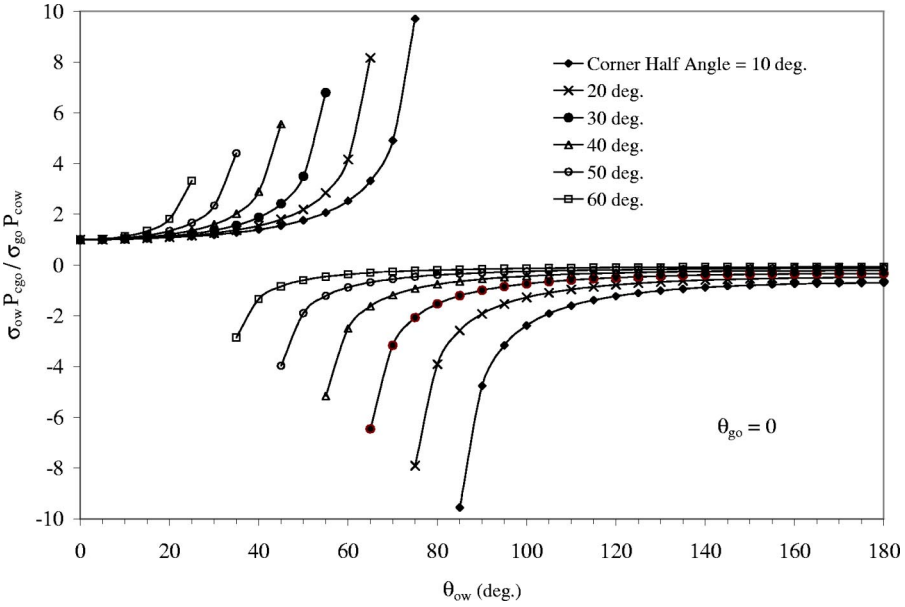

FIG. 9. Effects of corner half angle and oil/water contact angle on oil layer stability for $\theta_{go}=0$.

B. In these circumstances the displacement is purely a two-phase one. But if the gas in the center contacts the water in the corners then the threshold gas/oil capillary pressure becomes sensitive to oil/water capillary pressure, systems *C*, *D*, and *E*, and is not the same as the two-phase threshold capillary pressure anymore. This, for instance, may happen in nonspreading systems where the oil layers either do not form or are less stable.

We also showed how to take into account contact angle hysteresis, for instance, the gas/oil contact angle during oil invasion into gas.

The majority of the three-phase pore-scale network models [8,10,17,47–52] use two-phase threshold capillary pressures for three-phase displacements. But as mentioned earlier this is not a correct assumption in all circumstances and can introduce significant errors in the ranking of the displacements in network modeling. Network models carry out a series of displacements in order of threshold capillary pressure, and any change in these values translates into a change in the rank of the displacements, which in turn may affect the fluid arrangements in the porous medium.

ACKNOWLEDGMENTS

The members of the Imperial College Consortium on Pore-Scale Modelling (BG, BHP, JOGMEC, Schlumberger, Shell, Statoil, Saudi Aramco, Eni, Total, and the U.K. Department of Trade and Industry) are thanked for their financial support. We also thank K. S. Sorbie and M. I. J. van Dijke (Heriot-Watt University), P. E. Øren (Statoil), and M. Araujo (Imperial College London) for their valuable comments.

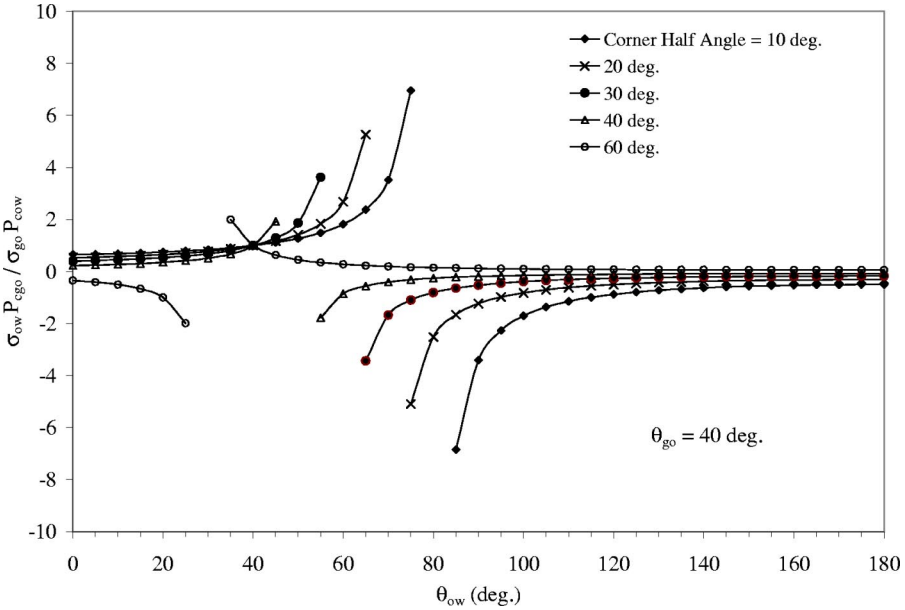

FIG. 10. Effects of corner half angle and oil/water contact angle on oil layer stability for $\theta_{go}=40$ deg.

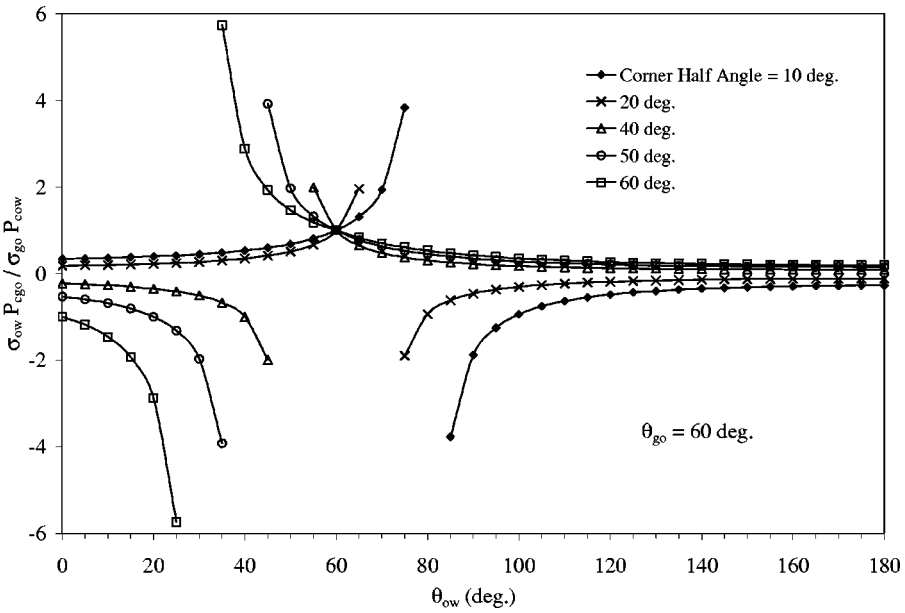

FIG. 11. Effects of corner half angle and oil/water contact angle on oil layer stability for $\theta_{go}=60$ deg.

APPENDIX A: USEFUL GEOMETRICAL RELATIONSHIPS FOR TRIANGLES

An irregular triangle with the corner half angles α_1, α_2, and α_3 and the convention of $0 \leqslant \alpha_1 \leqslant \alpha_2 \leqslant \alpha_3 \leqslant \pi/2$ (see Fig. 12) is considered. α_1 and α_2 are two corner half angles associated with the base of the triangle and R is the inscribed radius which is related to the area A and perimeter L of the element through [5]

$$R = \frac{2A}{L} = 2LG \tag{A1}$$

where G is the shape factor, which is the area divided by the perimeter squared, A/L^2.

Since the cross section is a composition of six triangles with equal size of R (see Fig. 12), from elementary geometry A is given by [53]

$$A = \frac{R^2}{4G} = R^2 \sum_{i=1}^{3} \cot \alpha_i. \tag{A2}$$

Since $\alpha_3 = \pi/2 - \alpha_1 - \alpha_2$,

$$G = \frac{1}{4}\left[\sum_{i=1}^{3} \cot \alpha_i\right]^{-1} = \frac{1}{4} \tan \alpha_1 \tan \alpha_2 \cot(\alpha_1 + \alpha_2). \tag{A3}$$

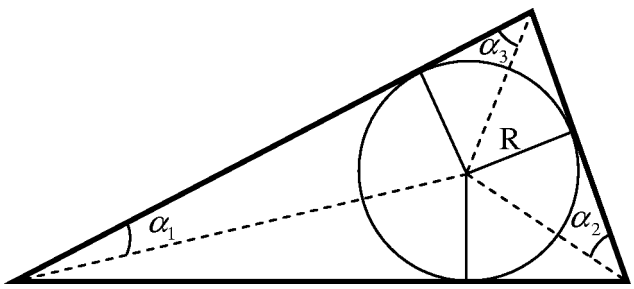

FIG. 12. An element with irregular triangular cross section.

The shape factor for irregular triangles ranges from zero corresponding to a slitlike element to $\sqrt{3}/36 \approx 0.0481$ belonging to equilateral triangles. A given value of G corresponds to a range of triangles where the limits of the range are denoted by $\alpha_{2,min}$ and $\alpha_{2,max}$, which in turn correspond to the triangles where $\alpha_{2,min} = \alpha_1 = \alpha$ and $\alpha_{2,max} = \pi/4 - \alpha_1/2$. The shape factor is related to $\alpha_{2,min}$ and $\alpha_{2,max}$ by [5,6]

$$G = \frac{1}{4}\left[\frac{2}{\tan \alpha_{2,min}} + \tan(2\alpha_{2,min})\right]^{-1}, \tag{A4}$$

$$G = \frac{\sin(2\alpha_1)}{2}\left[2 + \frac{\sin(2\alpha_1)}{\sin(2\alpha_{2,max})}\right]^{-2} = \frac{\sin(2\alpha_{2,max})\cos(2\alpha_{2,max})}{4[1 + \cos(2\alpha_{2,max})]^2}. \tag{A5}$$

In a triangle, for a given G the value of α_2 is selected randomly ($\alpha_{2,min} \leqslant \alpha_2 \leqslant \alpha_{2,max}$). Then Eq. (A3) is used to find

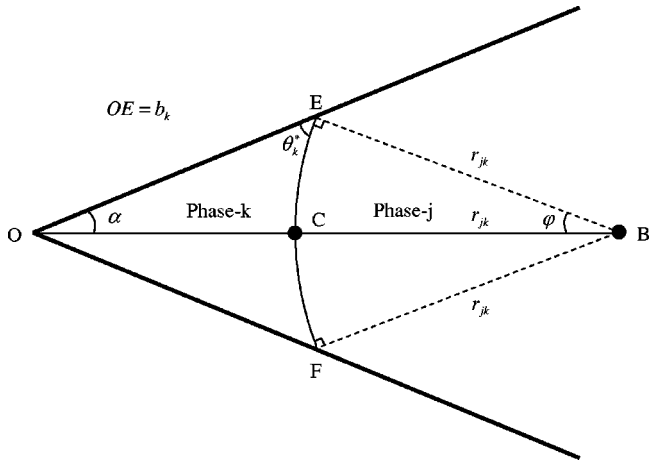

FIG. 13. An interface in a corner separating phases k and j.

the corresponding value of α_1. And finally $\alpha_3 = \pi/2 - \alpha_1 - \alpha_2$.

APPENDIX B: AREA AND MENISCUS-APEX DISTANCE OF AN INTERFACE IN A CORNER

Figure 13 shows a single corner of a capillary element where the wetting fluid resides in the corner and the nonwetting phase in the center. Here we derive the expressions to calculate the area occupied by the fluid in the corner, $A_{k,\measuredangle}$, and also the meniscus-apex distance of the interface, b_k. Consider the triangle *OEB*:

$$\frac{r_{jk}}{\sin\alpha} = \frac{b_k}{\sin\varphi}, \tag{B1}$$

$$\varphi = \pi - \left(\theta_k^* + \frac{\pi}{2}\right) - \alpha,$$

$$\varphi = \frac{\pi}{2} - (\theta_k^* + \alpha). \tag{B2}$$

From Eqs. (B1) and (B2),

$$b_k = r_{jk}\frac{\cos(\theta_k^* + \alpha)}{\sin\alpha}. \tag{B3}$$

Now we derive an expression for the area occupied by phase k in the corner, $A_{k,\measuredangle}$. Consider triangle *OEB*:

$$A_{OEB} = \frac{b_k}{2} OB \sin\alpha, \tag{B4}$$

$$\frac{r_{jk}}{\sin\alpha} = \frac{OB}{\sin[\pi - (\theta_k^* + \pi/2)]}, \tag{B5}$$

$$OB = \frac{r_{jk}}{\sin\alpha}\cos\theta_k^*, \tag{B6}$$

$$A_{OEB} = \frac{r_{jk}^2\cos(\alpha + \theta_k^*)}{2\sin\alpha}\cos\theta_k^*. \tag{B7}$$

Then from elementary geometry

$$A_{BEF} = r_{jk}^2\varphi = r_{jk}^2\left[\frac{\pi}{2} - (\theta_k^* + \alpha)\right], \tag{B8}$$

$$\begin{aligned} A_{k,\measuredangle} &= A_{OEF} \\ &= 2A_{OEB} - A_{BEF} \\ &= r_{jk}^2\left\{\frac{\cos(\alpha + \theta_k^*)}{\sin\alpha}\cos\theta_k^* - \left[\frac{\pi}{2} - (\theta_k^* + \alpha)\right]\right\}. \end{aligned} \tag{B9}$$

Also the length of the contact line between phases j and k is given by

$$L_{jk} = 2r_{jk}\varphi = 2r_{jk}\left[\frac{\pi}{2} - (\theta_k^* + \alpha)\right]. \tag{B10}$$

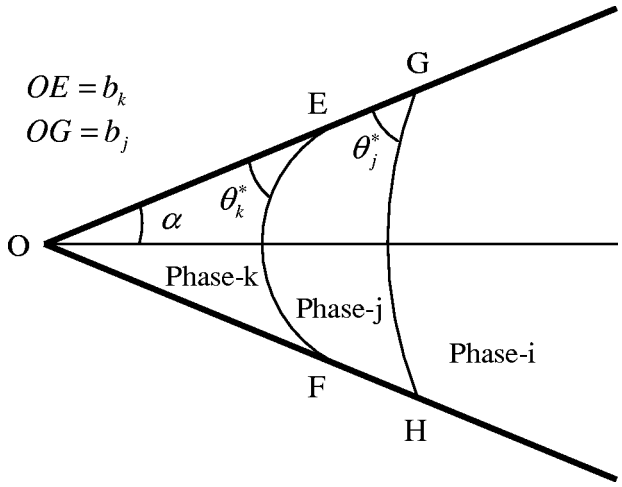

FIG. 14. A corner with phases k, j, and i residing in corner, layer, and center, respectively.

It is also possible to have one or even two layers residing in the corner (see Fig. 2). In Fig. 14 the area occupied by fluid j in layer, $A_{j,\measuredangle}$, and the meniscus-apex distance of the interface creating the layer, b_j, are found in a similar way:

$$b_j = r_{ij}\frac{\cos(\theta_j^* + \alpha)}{\sin\alpha},$$

$$A_{j,\measuredangle} = A_{EFHG} = r_{ij}^2\left\{\frac{\cos(\alpha + \theta_j^*)}{\sin\alpha}\cos\theta_j^* - \left[\frac{\pi}{2} - (\theta_j^* + \alpha)\right]\right\} - A_{k,\measuredangle} \tag{B11}$$

where $A_{k,\measuredangle}$ is given by Eq. (B9).

APPENDIX C: LAYER COLLAPSE

Pistonlike displacements—if the pertinent contact angles, capillary pressures, and corner half angles permit—allow the displaced phase to remain as layer(s) sandwiched between fluids in the corner(s) and center of the element. The layers may spontaneously collapse by an increase in pressure of the fluids on either side of the layer. When a layer collapse event takes place, one of the two AMs bounding the layer will hinge and/or move toward the other one. However, there are cases where both AMs contribute to the layer collapse event, e.g., oil layer collapse by water in a strongly oil-wet element (see configuration *D* in Fig. 2).

Based on whether the fluids residing on the two sides of the layer are the same, layers may be categorized into two main groups: (I) identical fluids; (II) different fluids. Here, the stability of the layers, i.e., the threshold capillary pressure for layer collapse and formation events, in each category is discussed [10,45,46].

1. Identical fluids on two sides of a layer

Figure 15 illustrates this case. Since fluids residing on both sides of the layer are identical, when the capillary pressure of the fluid pair changes both bounding AMs contribute

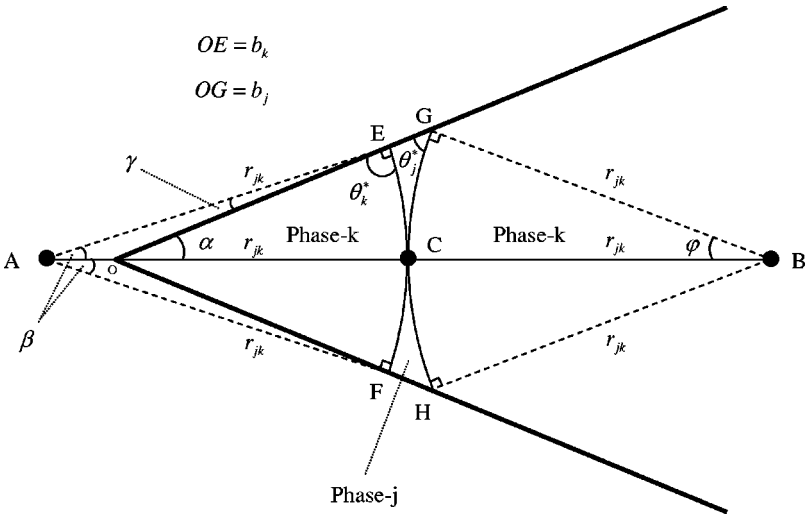

FIG. 15. A layer sandwiched between identical fluids residing in the corner and center.

to the stability of the layer. The layer stays stable until two AMs touch each other at point *C* when the layer collapses immediately and the corner is filled completely by phase *k*. This is the concept that is used here to derive an expression for threshold capillary pressure of collapse of such a layer (note: the expression given by Hui and Blunt [45] for this capillary event is incorrect).

Using Eq. (B6) we obtain

$$OC = OB - r_{jk} = r_{jk}\left[\frac{\cos\theta_j^*}{\sin\alpha} - 1\right]. \tag{C1}$$

Consider triangle *AOE*:

$$\frac{r_{jk}}{\sin(\pi-\alpha)} = \frac{b_k}{\sin\beta}, \tag{C2}$$

$$\sin(\pi-\alpha) = \sin\alpha;$$

therefore

$$\sin\beta = \frac{b_k}{r_{jk}}\sin\alpha, \tag{C3}$$

$$\gamma = \pi - (\pi-\alpha) - \beta = \alpha - \beta. \tag{C4}$$

Also,

$$\frac{AO}{\sin\gamma} = \frac{b_k}{\sin\beta}. \tag{C5}$$

From Eqs. (C3), (C4) and (C5),

$$\frac{AO}{\sin(\alpha-\beta)} = \frac{r_{jk}}{\sin\alpha}, \tag{C6}$$

$$AO = \frac{r_{jk}}{\sin\alpha}\sin(\alpha-\beta) = \frac{r_{jk}}{\sin\alpha}(\sin\alpha\cos\beta - \cos\alpha\sin\beta). \tag{C7}$$

From Eqs. (C3) and (C7),

$$AO = r_{jk}\cos\beta - b_k\cos\alpha, \tag{C8}$$

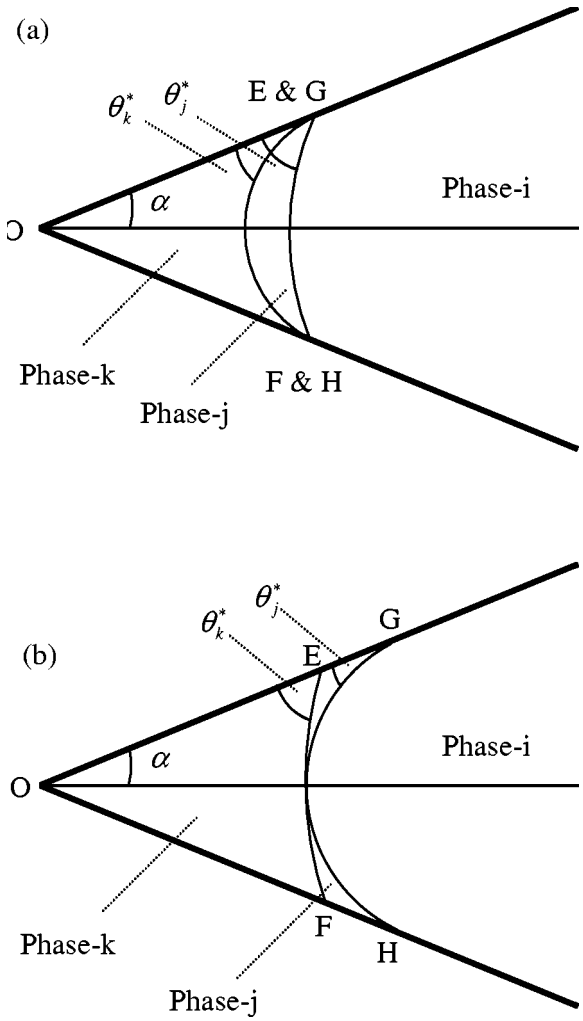

FIG. 16. A layer sandwiched between different fluids residing in the corner and center. Position of the AMs at the moment of collapse when (a) $\theta_k^* < \theta_j^*$; (b) $\theta_k^* > \theta_j^*$.

$$OC = r_{jk} - AO, \tag{C9}$$

$$OC = r_{jk} - r_{jk}\cos\beta + b_k\cos\alpha. \tag{C10}$$

From equating Eqs. (C1) and (C10):

$$r_{jk}\left(2 - \frac{\cos\theta_j^*}{\sin\alpha}\right) + b_k\cos\alpha = r_{jk}\cos\beta, \tag{C11}$$

$$r_{jk}^2\left(4 - 4\frac{\cos\theta_j^*}{\sin\alpha} + \frac{\cos^2\theta_j^*}{\sin^2\alpha}\right) + b_k^2\cos^2\alpha + 2b_k r_{jk}\cos\alpha\left(2 - \frac{\cos\theta_j^*}{\sin\alpha}\right) = r_{jk}^2\cos^2\beta, \tag{C12}$$

$$\begin{aligned} r_{jk}^2\cos^2\beta &= r_{jk}^2(1-\sin^2\beta) \\ &= r_{jk}^2\left(1 - \frac{b_k^2}{r_{jk}^2}\sin^2\alpha\right) \\ &= r_{jk}^2 - b_k^2\sin^2\alpha, \end{aligned} \tag{C13}$$

$$r_{jk}^2\left(3 - 4\frac{\cos\theta_j^*}{\sin\alpha} + \frac{\cos^2\theta_j^*}{\sin^2\alpha}\right) + 2b_k r_{jk}\cos\alpha\left(2 - \frac{\cos\theta_j^*}{\sin\alpha}\right) + b_k^2 = 0, \tag{C14}$$

$$r_{jk} = \frac{-2b_k\cos\alpha[2 - (\cos\theta_j^*/\sin\alpha)] \pm M}{[6 - 8(\cos\theta_j^*/\sin\alpha) + 2(\cos^2\theta_j^*/\sin^2\alpha)]}, \tag{C15}$$

$$M = \left[4b_k^2\cos^2\alpha\left(4 - 4\frac{\cos\theta_j^*}{\sin\alpha} + \frac{\cos^2\theta_j^*}{\sin^2\alpha}\right) - 12b_k^2 + 16b_k^2\frac{\cos\theta_j^*}{\sin\alpha} - 4b_k^2\frac{\cos^2\theta_j^*}{\sin^2\alpha}\right]^{1/2}, \tag{C16}$$

$$\frac{r_{jk}}{b_k} = \frac{-2\sin^2\alpha\cos\alpha + \cos\alpha\sin\alpha\cos\theta_j^* \pm N}{3\sin^2\alpha - 4\sin\alpha\cos\theta_j^* + \cos^2\theta_j^*}, \tag{C17}$$

$$N = [4\cos^2\alpha\sin^4\alpha - 4\sin^3\alpha\cos\theta_j^*\cos^2\alpha + \cos^2\alpha\sin^2\alpha\cos^2\theta_j^* - 3\sin^4\alpha + 4\cos\theta_j^*\sin^3\alpha - \cos^2\theta_j^*\sin^2\alpha]^{1/2}, \tag{C18}$$

$$\frac{r_{jk}}{b_k} = \frac{-\cos\alpha\sin\alpha(2\sin\alpha - \cos\theta_j^*) \pm \sin^2\alpha[4\sin\alpha\cos\theta_j^* - 3 + 4\cos^2\alpha - \cos^2\theta_j^*]^{1/2}}{3\sin^2\alpha - 4\sin\alpha\cos\theta_j^* + \cos^2\theta_j^*}, \tag{C19}$$

$$P_{cjk} = -\frac{\sigma_{jk}}{r_{jk}}. \tag{C20}$$

Using Eq. (B3) we obtain

$$P_{cjk} = \frac{P_{cjk}^{ext}(3\sin^2\alpha + 4\sin\alpha\cos\theta_j^* + \cos^2\theta_j^*)}{\cos(\theta_k^* + \alpha)[\cos\alpha(2\sin\alpha - \cos\theta_j^*) + \sin\alpha\sqrt{4\cos^2\alpha - 3 - \cos^2\theta_j^* + 4\sin\alpha\cos\theta_j^*}]} \tag{C21}$$

where P_{cjk}^{ext} and θ_k^* are the capillary pressure and the angle of the last move of the interface between phase k in the corner and phase j in the layer.

2. Different fluids on two sides of a layer

Since the layer is surrounded by two different fluids, a change in the pressure of either fluids can result in layer collapse. Depending on the magnitude of the angle that each AM makes with the wall, two main groups of collapse scenario are possible.

a. $\theta_k^* \leqslant \theta_j^*$

Figure 16(a) illustrates the case. The stability of the layer depends on the ratio of the curvature of the two AMs bounding the layer

$$\frac{r_{jk}}{r_{ij}} = \frac{\sigma_{jk}P_{cij}}{\sigma_{ij}P_{cjk}} \tag{C22}$$

where σ_{jk} and σ_{ij} are the interfacial tensions of the bounding interfaces of the layer and P_{cjk} and P_{cij} are pertinent capillary pressures. The layer is stable until three-phase contact points meet each other [see Fig. 16(a)]. This means that the layer collapses when the meniscus-apex distances b for two AMs become equal. The layer is stable if

$$\frac{r_{jk}}{r_{ij}} \leqslant \frac{\cos(\theta_j^* + \alpha)}{\cos(\theta_k^* + \alpha)}. \tag{C23}$$

b. $\theta_k^* > \theta_j^*$

Figure 16(b) illustrates this case. The layer is stable until two AMs meet at their centers. The ratio of curvature of two AMs at the collapsing point is found by equating the center-

apex distance of one of the AMs to that of the other one. The layer is stable if

$$\frac{r_{jk}}{r_{ij}} \leqslant \frac{\sin\alpha - \cos\theta_j^*}{\sin\alpha - \cos\theta_k^*}. \tag{C24}$$

One should note that if the curvature of any of the AMs is negative (see Fig. 2), the threshold capillary pressures for layer collapse are found using the same procedure as above. It is also possible to have a second layer sandwiched between the fluids residing in the center of the element and the first layer (see Fig. 2). The stability analysis for the second layer is also the same as that of the first layer.

[1] M. A. Celia, P. C. Reeves, and L. A. Ferrand, Rev. Geophys. **33**, 1049 (1995).
[2] M. J. Blunt, Curr. Opin. Colloid Interface Sci. **6**, 197 (2001).
[3] M. J. Blunt, M. D. Jackson, M. Piri, and P. H. Valvatne, Adv. Water Resour. **25**, 1069 (2002).
[4] R. Ehrlich and D. K. Davies, Proceedings of the SPE Gas Technology Symposium, Dallas, Texas 1989, Paper SPE 19054.
[5] G. Mason and N. R. Morrow, J. Colloid Interface Sci. **141**, 262 (1991).
[6] P. E. Øren, S. Bakke, and O. J. Arntzen, SPEJ **3**, 324 (1998).
[7] T. W. Patzek, SPEJ **6**, 144 (2001).
[8] M. I. J. van Dijke and K. S. Sorbie, Phys. Rev. E **66**, 046302 (2002).
[9] D. H. Fenwick and M. J. Blunt, SPEJ **3**, 86 (1998).
[10] D. H. Fenwick and M. J. Blunt, Adv. Water Resour. **21**, 121 (1998).
[11] J. K. Larsen, N. Bech, and A. Winter, Proceedings of the SPE/DOE Improved Oil Recovery Symposium, Tulsa, Oklahoma, 2000, Paper SPE 59324.
[12] P. A. Goode and T. S. Ramakrishnan, AIChE J. **39**, 1124 (1993).
[13] H. N. Man and X. D. Jing, J. Pet. Sci. Eng. **24**(2-4), 255 (1999).
[14] G. G. Pereira, W. V. Pinczewski, D. Y. C. Chan, L. Paterson, and P. E. Øren, Transp. Porous Media **24**, 167 (1996).
[15] R. Lenormand, C. Zarcone, and A. Sarr, J. Fluid Mech. **135**, 337 (1983).
[16] R. Lenormand and C. Zarcone, Proceedings of the 59th SPE Annual Technical Conference and Exhibition, Houston, Texas, 1984, Paper SPE 13264.
[17] M. Piri and M. J. Blunt, Phys. Rev. E (to be published).
[18] R. P. Mayer and R. A. Stowe, J. Colloid Sci. **20**, 893 (1965).
[19] H. M. Princen, J. Colloid Interface Sci. **30**, 69 (1969).
[20] H. M. Princen, J. Colloid Interface Sci. **30**, 359 (1969).
[21] H. M. Princen, J. Colloid Interface Sci. **34**, 171 (1970).
[22] B. Legait, J. Colloid Interface Sci. **96**, 28 (1983).
[23] N. R. Morrow, Proceedings of the First International Symposium on Evaluation of Reservoir Wettability and Its Effect on Oil Recovery, Socorro, New Mexico, 1990.
[24] S. Ma, G. Mason, and N. R. Morrow, Colloids Surf., A **117**, 273 (1996).
[25] M. Lago and M. Araujo, J. Colloid Interface Sci. **243**, 219 (2001).
[26] M. Lago and M. Araujo, Physica A **319**, 175 (2003).
[27] M. I. J. van Dijke and K. S. Sorbie, J. Colloid Interface Sci. **260**, 385 (2003).
[28] M. I. J. van Dijke, M. Lago, K. S. Sorbie, and M. Araujo, J. Colloid Interface Sci. **277**, 184 (2004).
[29] M. I. J. van Dijke and K. S. Sorbie, Proceedings of the International Conference on Computational Methods in Water Resources, Chapel Hill, North Carolina, 2004.
[30] A. W. Adamson and A. P. Gast, *Physical Chemistry of Surfaces*, 6th ed. (John Wiley and Sons, New York, 1997).
[31] J. S. Rowlinson and B. Widom, *Molecular Theory of Capillarity*, 1st ed. (Dover, New York, 1982).
[32] N. R. Morrow, H. T. Lim, and J. S. Ward, Heat./Piping/Air Cond. **2**, 89 (1986).
[33] O. Fassi-Fihri, M. Robin, and E. Rosenberg, Proceedings of the 66th SPE Annual Technical Conference and Exhibition, Dallas, Texas, 1991, Paper SPE 22596.
[34] A. R. Kovscek, H. Wong, and C. J. Radke, AIChE J. **39**, 1072 (1993).
[35] J. S. Buckley, Y. Liu, and S. Monsterleet, SPEJ **3**, 54 (1998).
[36] L. W. Lake, *Improved Oil Recovery* (Prentice-Hall, Englewood Cliffs, NJ, 1989).
[37] N. R. Morrow, J. Can. Pet. Technol. **14**, 42 (1975).
[38] N. R. Morrow, J. Can. Pet. Technol. **15**, 49 (1976).
[39] S. Ono and S. Kondo, *Handbook of Chemistry and Physics*, Vol. 10 , (RC, Boca Raton, FL, 1960), p. 134.
[40] J. W. Gibbs, *The Collected Works* (Longmans, Green and Co., New York, 1928), Vol. I.
[41] A. Firoozabadi, *Thermodynamics of Hydrocarbon Reservoirs* (McGraw-Hill, New York, 1999).
[42] F. E. Bartell and H. J. Osterhoff, Ind. Eng. Chem. **19**, 1277 (1927).
[43] D. Zhou and M. J. Blunt, J. Contam. Hydrol. **25**, 1 (1997).
[44] M. J. Blunt, J. Colloid Interface Sci. **239**, 281 (2001).
[45] M. H. Hui and M. J. Blunt, J. Phys. Chem. B **104**, 3833 (2000).
[46] T. Firincioglu, M. J. Blunt, and D. Zhou, Colloids Surf., A **155**, 259 (1999).
[47] M. Piri and M. J. Blunt, Phys. Rev. E (to be published).
[48] W. E. Soll and M. A. Celia, Adv. Water Resour. **16**, 107 (1993).
[49] P. E. Øren, J. Billiotte, and W. V. Pinczewski, Proceedings of the SPE/DOE Symposium in Improved Oil Recovery, Tulsa, Oklahoma, 1994, Paper SPE 27814.
[50] V. Mani and K. K. Mohanty, SPEJ **3**, 238 (1998).
[51] T. R. Lerdahl, P. E. Øren, and S. Bakke, Proceedings of the SPE/DOE Symposium in Improved Oil Recovery, Tulsa, Oklahoma, 2000, Paper SPE 59311.
[52] M. Piri and M. J. Blunt, Proceedings of the SPE Annual Technical Conference and Exhibition, San Antonio, Texas, 2002, Paper SPE 77726.
[53] T. W. Patzek and D. B. Silin, J. Colloid Interface Sci. **236**, 295 (2001).